Size-Dependent Binding Energies of Methane to Small Gold Clusters

Sandra M. Lang,[a] Thorsten M. Bernhardt,*[a] Robert N. Barnett,[b] and Uzi Landman*[b]

Dedicated to Prof. Dr. R. Jürgen Behm on the occasion of his 60th birthday

The reactions of small gold cluster cations Au_x^+ ($x = 2$–6) with CH_4 were studied by joint gas-phase kinetics and first-principles density functional theory calculations. The experimentally obtained temperature-dependent low pressure rate constants were analyzed by employing the Lindemann energy transfer model for association reactions in conjunction with statistical RRKM theory. In this way cluster-size-dependent binding energies of methane to the gold cluster cations were determined from the experimental data for two different transition-state models. The experimental binding energies obtained by employing a "loose" transition-state model are in good agreement with the theoretical values at the optimal adsorption geometries, while a "tight" transition-state model clearly gives a lower limit for the binding energies. Additionally, Kohn–Sham molecular orbitals of Au_x–CH_4^+ are presented to gain detailed insight into the cluster–methane bonding mechanism.

1. Introduction

Gas-phase studies of free metal clusters provide an ideal means to investigate, at a strictly molecular level, the energetics and kinetics of bond-making and bond-breaking processes related to elementary steps potentially involved in reactions catalyzed by metal particles. As stated in a recent review, although such investigations might never account for the precise mechanisms, energetics, and kinetics operating in applied catalysis, gas-phase studies can provide a conceptual framework and an efficient tool to obtain direct insight into reactivity patterns.[1] Furthermore, by increasing the cluster size atom by atom, important knowledge about the transition from the chemistry of single atoms to that of nanoparticles can be obtained.[2]

In terms of reactivity patterns, quantitative knowledge about binding energies of relevant molecules to the metal clusters is of special importance as trends might be identified that would help to device or improve possible catalytic process involving clusters or nanoparticles.

From an economic point of view, the catalytic conversion of small hydrocarbons such as methane to more "valuable" products and the pertinent sigma bond activation is of particular interest.[3] In previous studies, the activation and dehydrogenation of methane, yielding the product MCH_2^+, has been observed for a variety of third-row transition metal cations (M^+).[4,5] However, Au^+ was found previously to be among the few 5d metals that are completely unreactive toward methane.[5]

In contrast to the numerous experimental data on methane adsorption and activation on *atomic* transition metal ions, only few investigations concerning methane adsorption on cationic metal *clusters* are available. While small platinum clusters Pt_x^+ were found to be able to activate and dehydrogenate methane, yielding $Pt_xCH_2^+$ ($x \leq 9$) as well as $Pt_xC_2H_4^+$ ($x = 1, 5$),[6] the reactivity of the binary platinum–gold clusters $Pt_xAu_y^+$ de-

creased with increasing gold content. Consequently, pure gold clusters Au_x^+ were found to be completely unreactive toward CH_4 under the single-collision conditions employed in these experiments.[7] In contrast, an uptake of several CH_4 molecules was observed under multi-collision conditions.[8] Although dehydrogenation of CH_4 was not directly observed in the latter study, it was proposed that methane was dissociatively bound as methyl plus hydride (CH_3–Au_x^+–H). However, only recently a combined theoretical and experimental study[9] could directly prove that the positively charged gold dimer, Au_2^+, is able to adsorb methane, to activate it through coadsorption of a second molecule of CH_4, and, most surprisingly, to selectively catalyze the formation of ethylene at temperatures as low as 250 K.

Herein, we report a detailed temperature-dependent gas-phase reaction kinetics investigation and first-principles theoretical calculations revealing the adsorption and bonding mechanism of methane on a series of small gold cluster cations Au_x^+ with $x = 2$–6 atoms. Besides the reaction mechanisms, experimentally and theoretically obtained cluster-size-dependent methane binding energies to the gold cluster cations are presented for the first time. Furthermore, calculations of the optimal atomic adsorption geometries as well as of

[a] Dr. S. M. Lang, Prof. Dr. T. M. Bernhardt
Institute of Surface Chemistry and Catalysis
University of Ulm
Albert-Einstein-Allee 47, 89069 Ulm (Germany)
Fax: (+49)731-50-25452
E-mail: thorsten.bernhardt@uni-ulm.de

[b] Dr. R. N. Barnett, Prof. Dr. U. Landman
School of Physics
Georgia Institute of Technology
Atlanta, Georgia 30332-0430 (USA)
Fax: (+1)404-894-7747
E-mail: uzi.landman@physics.gatech.edu

Kohn–Sham molecular orbitals of $Au_x-CH_4^+$ ($x=2,6$) permit detailed insight into the cluster–methane binding mechanism.

Experimental Section

Experimental Setup: The experimental setup to study gold cluster ion reactions and to obtain temperature-dependent rate constants consists of a variable temperature radio frequency (rf) octopole ion trap inserted into a tandem quadrupole mass spectrometer.

The metal cluster cations are produced by a CORDIS (cold reflex discharge ion source)[10] sputtering ion source. Clusters are mass selected in a first quadrupole filter. The cluster ion beam containing only clusters of one specific mass then enters the octopole ion trap, which is prefilled with about 1 Pa partial pressure of helium buffer gas and a small, well defined fraction of CH_4. The ion trap enclosure is attached to a helium cryostat that allows for temperature adjustment in the range between 20 K and 300 K.

The absolute pressure inside the ion trap is measured by a Baratron gauge (MKS, Typ 627B) attached to the ion trap via a 1 mm inner diameter teflon tube. For exact pressure determination inside of the ion trap, however, it has to be taken into account that the Baratron capacitance manometer is thermally stabilized at 318 K, in contrast to the variable temperature ion trap. Thus, the effect of thermal transpiration has to be considered. Thermal transpiration leads, in its simplest form, to a correction factor[11] of $p_{trap}/p_{gauge} = (T_{trap}/T_{gauge})^{1/2}$, where p_{gauge} denotes the pressure read from the gauge, p_{trap} the true pressure inside the ion trap, T_{gauge} the Baratron gauge temperature (318 K), and T_{trap} the ion trap temperature. For a more detailed discussion see ref. [12].
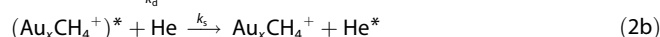
At the applied pressures, thermal equilibration of the clusters with the buffer gas is achieved within a few milliseconds,[13] whereas the cluster ions are typically stored in the ion trap for several seconds. After a chosen reaction time, all ionic reactants, intermediates, and products are extracted from the ion trap, and the ion distribution is analyzed via a second quadrupole mass filter. By recording all ion intensities as a function of the reaction time t_R, the rates of the reaction at a well defined reaction temperature can be studied. More details of the experimental setup are given in refs. [13, 14].

Data Evaluation: The data evaluation procedure applied to analyze the temperature-dependent kinetic traces and the corresponding error analysis has been described in great detail elsewhere[12] and is only briefly summarized here. The normalized kinetic traces are evaluated by fitting the integrated rate equations of proposed potential reaction mechanisms to the experimental data by using the "*Detmech*" software.[15] This leads to the determination of the simplest reaction mechanism that best fits the experimental data and yields pseudo-first order reaction rate constants k (the concentration of methane and of the helium buffer gas can be considered constant with respect to the metal cluster concentration[13, 16]). As an example, the simple association reaction given by Equation (1):

$$Au_x^+ + CH_4 \xrightarrow{k} Au_xCH_4^+ \tag{1}$$

of the a gold cation Au_x^+ with one methane molecule is examined in the following. Nevertheless, also for more complicated reaction mechanisms the elementary models discussed below apply to all individual reaction steps.

Because the experiments were performed at about 1 Pa total pressure and thus in the kinetic low-pressure regime, the details of Equation (1) can be described by the Lindemann energy transfer model for association reactions[16] which is represented by Equations (2a,b):

$$Au_x^+ + CH_4 \underset{k_d}{\overset{k_a}{\rightleftharpoons}} Au_xCH_4^{+*} \tag{2a}$$

$$(Au_xCH_4^+)^* + He \xrightarrow{k_s} Au_xCH_4^+ + He^* \tag{2b}$$

According to this model, the gold cation Au_x^+ reacts with the CH_4 molecule, forming the energized intermediate $(Au_xCH_4^+)^*$ with a rate constant k_a. This intermediate may decompose unimolecularly back to the reactants (rate constant k_d) or may be stabilized by an energy-transfer collision with helium buffer gas (rate constant k_s). Consequently, the overall Equation (1) depends on the helium buffer gas and becomes of third order. The corresponding measured pseudo-first order rate constant k is then given by Equation (3):

$$k = k^{(3)}[He][CH_4] \tag{3}$$

and contains the termolecular rate constant [Eq. (4)]:

$$k^{(3)} = \frac{k_a k_s}{k_d} \tag{4}$$

The ion–molecule association rate constant k_a and the stabilization rate constant k_s are approximated by ion–molecule collision rate constants as specified by Langevin theory.[16,17] In ion mobility measurements it was shown that this model oversimplifies the cluster size effect,[18] however a more precise determination of these rate constants using cluster-size-dependent cross sections was not possible due to the lack of available experimental literature data. Since both neutral molecules, CH_4 and He, are nonpolar molecules, the rate constants k_a and k_s are temperature independent.[16] Therefore, any observed temperature dependence of Equation (1) must be contained in the unimolecular decomposition rate constant k_d.

Combining Equations (2)–(4) allows for the determination of an experimental unimolecular decomposition rate constant k_d of the energized complex $(Au_xCH_4^+)^*$. This rate constant is also well described by RRKM (Rice–Ramsperger–Kassel–Marcus) theory.[19,20] According to this theory the decomposition reaction step is considered to proceed via Equation (5):

$$(Au_xCH_4^+)^* \xrightarrow{k_d} (Au_xCH_4^+)^+ \rightarrow Au_x^+ + CH_4 \tag{5}$$
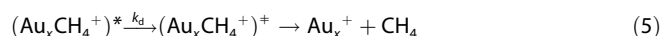
involving the energized complex $(Au_xCH_4^+)^*$ and the transition state $(Au_xCH_4^+)^+$. RRKM theory is usually applied to determine k_d from the known binding energy of the ligand to the cluster ion. In our experimental approach k_d is the quantity derived from the experimental data, which consequently allows for the determination of the binding energy. In order to obtain RRKM binding energies E_0, the experimental decomposition rate constants k_d have been simulated using the software package "*MassKinetics*" developed by Drahos et al.[12,21]

Theoretical Methods: Our theoretical explorations of the atomic arrangements and electronic structures of the Au_x^+ clusters and of their binding with methane were performed with the use of density functional theory (DFT) calculations. In particular, we employed the Born–Oppenheimer (BO)–spin density functional (SDF)–molecular dynamics (MD) method (BO–SDF–MD)[22] with norm-conserving soft pseudopotentials[23] (including a scalar relativistic pseudopotential[24] for Au) and the generalized gradient approximation (GGA)[25] for electronic exchange and correlations. In these calculations we used a plane wave basis with a kinetic energy cutoff of 62 Ry. The BO–SDF–MD method is particularly suitable for investigations of charged systems since it does not employ a supercell (i.e. no periodic replication of the ionic system is used). Uncon-

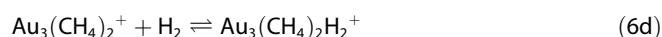strained structural optimizations were performed using a conjugate-gradient-like method.

2. Results and Discussion

2.1. Reaction Kinetics of the CH$_4$ Adsorption

For all investigated gold cluster cations Au$_x^+$ ($x=2$–6) gas-phase reaction kinetics were measured at ion trap temperatures of 270 K and of 250 K. At lower temperatures, most of the reactions proceeded so fast that the measurement of reaction-time-dependent product ion signals was impossible even at low CH$_4$ partial pressure. For Au$_2^+$, Au$_3^+$, and Au$_5^+$ additional measurements were performed at 300 K, while for Au$_4^+$ and Au$_6^+$ the intensity of the reaction products was too small to obtain kinetic data at this temperature.

It has to be noted that, in the experiments presented herein, besides CH$_4$ and helium buffer gas, trace amounts of H$_2$ [p(H$_2$) beyond the Baratron detection limit of 0.01 Pa] were also present in the ion trap due to impurities in the methane gas. However, in the investigated temperature range and under the given partial pressure conditions the methane uptake was faster than the hydrogen uptake. Thus, the kinetics of the CH$_4$ adsorption, especially of the first CH$_4$ molecule, was not influenced by H$_2$, which was only coadsorbed at longer reaction times.[29]

Figure 1 shows, as an example, selected mass spectra and kinetic data (open symbols) for the reactions of Au$_3^+$ and of Au$_5^+$ with methane at 300 K. The solid lines in the kinetic plots, for example, for Au$_3^+$, were obtained by fitting the integrated rate equations of the following proposed reaction mechanism to Equations (6 a–d):

$$Au_3^+ + CH_4 \overset{k}{\rightleftarrows} Au_3CH_4^+ \tag{6a}$$

$$Au_3CH_4^+ + CH_4 \rightleftarrows Au_3(CH_4)_2^+ \tag{6b}$$

$$Au_3CH_4^+ + H_2 \rightleftarrows Au_3CH_4H_2 \tag{6c}$$

$$Au_3(CH_4)_2^+ + H_2 \rightleftarrows Au_3(CH_4)_2H_2^+ \tag{6d}$$

A similar reaction mechanism was also obtained as best fit for the gold cluster cations Au$_4^+$, Au$_5^+$, and Au$_6^+$. Similar to previous studies,[8] also under the present experimental conditions there was no direct experimental evidence for the activation of one or more methane molecules upon adsorption on the gold cations Au$_x^+$ ($x=3$–6).

In contrast, for the gold dimer the reaction mechanism differed from the one for the larger gold clusters because Au$_2^+$ was found to be the only cluster investigated that was able to activate and dehydrogenate methane and even facilitate the formation of ethylene in a full thermal catalytic cycle.[9] However, the dehydrogenation was only observed in cooperative action upon adsorption of a second methane molecule while there was no indication for the dehydrogenation of the first CH$_4$. Consequently, all the following discussions for the adsorption of a first CH$_4$ molecule on Au$_x^+$ ($x=3$–6) are also valid for
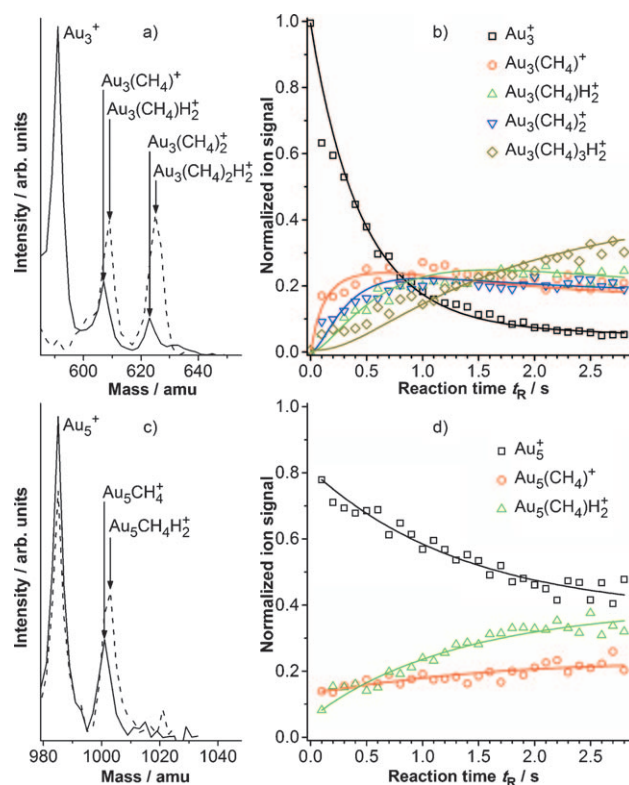
Figure 1. a) Mass spectra of the reaction Au$_3^+$ + CH$_4$ recorded after 0.1 s (——) and 2.0 s (-----) reaction times. b) Corresponding product ion concentrations as a function of the reaction time t_R. The open symbols represent the experimental data, normalized to the total ion concentration in the ion trap. The solid lines are obtained by fitting the integrated rate equations of the proposed reaction mechanism given by Equations (5 a–d) to the experimental data. c) Mass spectra of the reaction Au$_5^+$ + CH$_4$ recorded after 0.1 s (——) and 1.0 s (-----) reaction times. d) Corresponding product ion concentrations as a function of the reaction time t_R. Open symbols represent the experimental data, solid lines the kinetic fits. All data shown were obtained at 300 K. The corresponding partial pressures are listed in Table 1.

Au$_2^+$. A detailed report on the methane activation by Au$_2^+$ is given in a separate contribution.[9]

In order to obtain binding energies of a single methane molecule to the gold cluster cations, only the forward reaction step of Equation (5 a) [rate constant k], which corresponds to the formation of the complex Au$_x$CH$_4^+$, is considered in the following. For some of the investigated systems (Au$_3^+$ at 270 K and 250 K, Au$_5^+$ at 250 K), the adsorption of a first methane molecule was followed by the fast subsequent adsorption of a second or even a third methane molecule yielding the products Au$_x$(CH$_4$)$_y^+$ ($y=2,3$). Although, in these cases, the product Au$_x$CH$_4^+$ could not be detected on the time scale of our experiment, the adsorption of the first methane molecule represented the rate-determining step.[12] Thus, the fitted rate constant corresponds to the formation of Au$_x$CH$_4^+$.

All experimentally obtained temperature-dependent pseudo-first order (k) and termolecular ($k^{(3)}$) rate constants for the adsorption of the first CH$_4$ molecule onto Au$_x^+$ as well as the corresponding association rate constants k_a, the stabilization rate constants k_s, and the unimolecular decomposition

rate constants k_d are summarized in Table 1. The errors of k_d in Table 1 include the standard deviation resulting from the fitting procedure to obtain k and errors in the measured gas pressure, which are considered to be ± 0.01 Pa according to the detection limit of the Baratron gauge. For a detailed discussion of the error analysis, please refer to ref. [12]. All investigated cluster sizes exhibit a negative temperature dependence of $k^{(3)}$ and a corresponding positive temperature dependence of k_d [cf. also Eq. (2)]. This indicates a barrier-free CH_4 adsorption, which is typical for ion–molecule reactions.[16]

larger clusters were unknown. Thus, an estimation of the Au_x^+–CH_4 vibrational frequency using the Morse function model was not possible.

However, the available literature data on M–CH_4 vibrations for several different metal atoms M[27] all range between 417 cm^{-1} and 528 cm^{-1}. As copper is the only coinage metal investigated, the corresponding value of 434 cm^{-1} was thus taken in the calculations as an approximation for the Au_x^+–CH_4 vibration. To estimate the error of the computed RRKM binding energy E_0 resulting from this quite rough approximation, E_0 was calculated for three different values of the Au_3^+–CH_4 vibration. The deduced binding energies for a "tight" transition state (see below) are 0.39 $\pm$ 0.06 eV, 0.40 $\pm$ 0.06 eV, and 0.41 $\pm$ 0.06 eV for vibrational frequencies ν(Au$_3$–CH_4^+) of 350 cm^{-1}, 434 cm^{-1}, and 550 cm^{-1}, respectively. Hence, the considerable variation of this vibrational frequency between 350 cm^{-1} and 550 cm^{-1} influences the binding energies only to a minor extent, resulting in values that lie well within the error limits. Furthermore, the unknown bending vibrations[12] were chosen to be 50 cm^{-1}.

In the following, the binding energy E_0 was calculated by employing a "tight" and a "loose" transition state (TS). The "tight" transition state is usually associated with rearrangement processes and clearly gives a lower limit for the binding energy.[32] In this model, the vibrational frequencies are the same as for the energized molecule minus the Au_x^+–CH_4 vibration that is treated as internal translation along the reaction coordinate.

In contrast, the "loose" TS is commonly used to model simple bond cleavage reactions and thus, represents a more realistic model for the investigated Au_x^+-CH_4 systems. For the "loose" TS the low frequency bending vibrations (50 cm^{-1}) were scaled by a factor $f = 0.5$ in addition to the removal of the Au_x^+–CH_4 vibration.[12,33] This determination of the energized complex's vibrational frequencies is a rough approximation. However, not the exact frequencies but the distribution of frequencies is crucial (see also the discussion of the binding energy errors in ref. [12]).

All vibrational frequencies employed for the energized molecules $(Au_xCH_4^+)^*$ as well as for the "loose" TS $(Au_xCH_4^+)^\ddagger$ are given in Table 2.

Furthermore, adiabatic rotations were taken into account by considering a "rotational barrier" E_{RB}.[12,20,21] E_{RB} was calculated from the Au_x^+–CH_4 distance of the energized molecule, represented by the equilibrium distance r_e [cf. $d_{(Au-C)}$ in Table 4], and the Au_x^+–CH_4 distance in the TS, represented by the capture

Table 1. Measured pseudo-first order (k) and termolecular ($k^{(3)}$) rate constants for the investigated reactions of the gold cluster cations Au_x^+ with methane, as well as deduced unimolecular decomposition rate constants (k_d) of the energized complexes $(Au_xCH_4^+)^*$ at various temperatures T_R. Also included are the experimental pressure conditions (not yet corrected for thermal transpiration) and the Langevin rate constants k_a and k_s.

Au_x^+	T_R [K]	p(He) [Pa]	p(CH$_4$) [Pa]	k [s^{-1}]	$k^{(3)}$ [10^{-28} cm^6 s^{-1}]	k_a [10^{-10} cm^3 s^{-1}]	k_s [10^{-10} cm^3 s^{-1}]	k_d [10^8 s^{-1}]
Au$_2^+$	250	1.02	0.04	3.0 $\pm$ 0.6	11 $\pm$ 4	9.611	5.324	4.7 $\pm$ 1.6
	270	1.00	0.04	2.1 $\pm$ 0.4	8.5 $\pm$ 2.9	9.611	5.324	6.0 $\pm$ 2.0
	300	0.96	0.08	2.9 $\pm$ 0.3	6.8 $\pm$ 1.1	9.611	5.324	7.5 $\pm$ 1.2
Au$_3^+$	250	0.95	0.04	10 $\pm$ 1	40 $\pm$ 12	9.549	5.315	1.3 $\pm$ 0.4
	270	0.99	0.04	1.8 $\pm$ 0.2	7.6 $\pm$ 2.2	9.549	5.315	6.7 $\pm$ 1.9
	300	1.00	0.08	2.1 $\pm$ 0.4	4.9 $\pm$ 1.2	9.549	5.315	10 $\pm$ 2
Au$_4^+$	250	1.02	0.04	12 $\pm$ 6	44 $\pm$ 25	9.517	5.311	1.1 $\pm$ 0.7
	270	1.04	0.04	3.0 $\pm$ 0.3	12 $\pm$ 3	9.517	5.311	4.3 $\pm$ 1.3
Au$_5^+$	250	1.03	0.04	1.8	67	9.498	5.308	0.76
	270	0.97	0.04	8.4 $\pm$ 1.7	35 $\pm$ 12	9.498	5.308	1.4 $\pm$ 0.5
	300	1.00	0.08	0.67 $\pm$ 0.13	1.5 $\pm$ 0.4	9.498	5.308	33 $\pm$ 8
Au$_6^+$	250	0.94	0.04	0.33 $\pm$ 0.10	1.3 $\pm$ 0.5	9.485	5.307	38 $\pm$ 16
	270	0.93	0.04	0.14 $\pm$ 0.04	0.61 $\pm$ 0.24	9.485	5.307	83 $\pm$ 33

2.2. Energized Complex and Transition States

For the determination of the unimolecular decomposition rate constants k_d the software package *MassKinetics*[21] is employed. In the simulations the specification of the vibrational frequencies of the energized complex $(Au_xCH_4^+)^*$ and of the transition state $(Au_xCH_4^+)^\ddagger$ are required. To our knowledge no experimental or theoretical data concerning the vibrational frequencies and binding energies of the gold–methane complexes have been reported so far, except for Au$_2$CH$_4^+$.[9] Thus, the necessary vibrations of the energized complexes $(Au_xCH_4^+)^*$ were estimated.

The gold cluster metal–metal vibrations were adopted from Ding et al.[26] and the nine methane vibrations from Shimanouchi.[28] To estimate the gold–ligand stretching vibrations, the potential along the reaction coordinate is commonly modeled by a Morse function.[12,30] For such a computation the theoretical or experimental binding energies of CH_4 to the gold cluster cations, Au_x^+–CH_4, as well as to the gold bulk surface, Au_{bulk}–CH_4, and the Au_{bulk}–CH_4 vibrational frequency are required. Methane only weakly interacts with gold surfaces with an adsorption energy of 14.5 $\pm$ 0.2 kJ mol^{-1}[31] and no measurements of the vibrational frequencies are available. Additionally, the sole calculation of an Au_x^+–CH_4 binding energy has been performed for Au$_2^+$ so far[9] while the binding energies to the

Table 2. Calculated and approximated frequencies for the energized complexes $(Au_xCH_4^+)^*$ and the "loose" TS $(Au_xCH_4^+)^\ddagger$. The numbers in parentheses denote degeneracies.

$Au_xCH_4^+$	$(Au_xCH_4^+)^*$ Vibrational frequencies [cm^{-1}]	$(Au_xCH_4^+)^\ddagger$ ("Loose" TS) Vibrational frequencies [cm^{-1}]
$Au_2CH_4^+$	128;[26] 434;[27] 2917, 1534 (2), 3019 (3), 1306 (3);[28] 50 (4)	128; 2917, 1534 (2), 3019 (3), 1306 (3); 25 (4)
$Au_3CH_4^+$	101 (2), 161;[26] 434;[27] 2917, 1534 (2), 3019 (3), 1306 (3);[28] 50 (5)	101 (2),161; 2917, 1534 (2), 3019 (3), 1306 (3); 25(5)
$Au_4CH_4^+$	14, 70 (2), 82, 123, 144;[26] 434;[27] 2917, 1534 (2), 3019 (3), 1306 (3);[28] 50 (5)	14, 70 (2), 82, 123, 144; 2917, 1534 (2), 3019 (3), 1306 (3); 25 (5)
$Au_5CH_4^+$	50, 17, 34, 66, 70, 96, 118, 151, 172;[26] 434;[27] 2917, 1534 (2), 3019 (3), 1306 (3);[28] 50 (5)	50, 17, 34, 66, 70, 96, 118, 151, 172; 2917, 1534 (2), 3019 (3), 1306 (3); 25 (5)
$Au_6CH_4^+$	3, 16, 27, 34, 56, 70, 76, 102, 114, 124, 144, 172;[26] 434;[27] 2927, 1534 (2), 3019 (3), 1306 (3);[28] 50 (5)	3, 16, 27, 34, 56, 70, 76, 102, 114, 124, 144, 172; 2927, 1534 (2), 3019 (3), 1306 (3); 25 (5)

only reported literature value for the binding of CH_4 to an extended Au(111) surface. This value amounts to 0.15 eV (14.5 ± 0.2 kJ mol^{-1}[31]). In contrast, applying a "tight" TS model, the binding energy of CH_4 to the cluster containing as few as six atoms already comes close to this value. However, it should again be emphasized that the binding energies determined by applying a "tight" TS model only represent lower limits.

radius r_c of the long-range potential between Au_x^+ and CH_4 [Eq. (7)]:[20, 34]

$$E_{RB} = \left(\frac{r_c^2}{r_e^2}\right)k_BT \qquad (7)$$

As discussed elsewhere,[12] E_{RB} is a function of the temperature, but this temperature effect on the binding energy E_0 is negligible. Thus, an average value of E_{RB} at $T_R = 270$ K amounting to 0.09 eV for Au_2^+ and Au_3^+ as well as 0.08 eV for Au_4^+, Au_5^+, and Au_6^+ was employed in the fitting procedure.

2.3. Cluster-Size-Dependent Experimental Methane Binding Energies
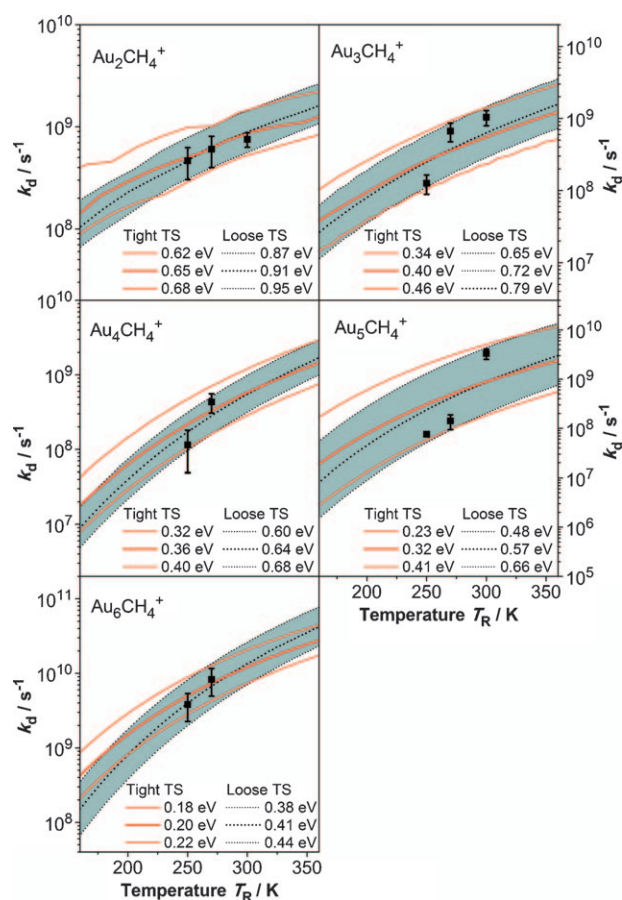
To illustrate the accuracy of the k_d fitting procedure, Figure 2 displays the experimentally obtained temperature-dependent unimolecular decomposition rate constants k_d (cf. also Table 1) together with the calculated RRKM $k_d(T_R)$ curves for both the "tight" (red curves) and "loose" (black curves, shaded areas) TSs. The mean value of the binding energy corresponds to a k_d vs T_R curve (bold lines) that best fits the experimental data. The additional lines represent estimated upper and lower limits to fit the experimental k_d values. Their corresponding E_0 values determine the reported uncertainties of the binding energies. These uncertainties include the errors in measuring k_d and fitting the RRKM rate constants.[12]

The cluster-size-dependent experimental RRKM binding energies for both "tight" and "loose" TSs (together with the theoretical binding energies; see below), are summarized in Table 3 and are illustrated in Figure 3. As mentioned above, the binding energies obtained by applying a "tight" TS represent lower limits and are about 0.3 eV lower compared to the "loose" TS binding energies.

From Figure 3 it can be seen that the binding energies decrease continuously with increasing cluster size for the same TS model. The largest binding energy of 0.65 ± 0.03 eV and 0.91 ± 0.04 eV for a "tight" and "loose" TS, respectively, was determined for Au_2^+.

The binding energies for all the investigated cluster sizes obtained by applying a "loose" TS model considerably exceed the

Figure 2. Experimental and RRKM decomposition rate constants k_d as a function of temperature. Solid squares represent the experimentally obtained temperature-dependent decomposition rate constants k_d. RRKM $k_d(T_R)$ curves computed for different binding energies E_0 are shown for a "tight" transition state (solid red lines) and for a "loose" transition state (doted black lines). Shown are the best fits to the experimental data (thick solid and dotted lines) and estimated upper and lower binding energy limits (thin solid lines and thin dotted lines). The wiggles apparent in some of the RRKM $k_d(T)$ curves are due to the stepwise calculation procedure required by the software and do not relate to a physical origin.

Table 3. Binding energies of CH$_4$ to all investigated gold cluster ions Au$_x^+$ as determined by employing RRKM theory for "tight" and "loose" TSs, respectively.

Au$_x^+$	E_0 [eV] "tight" TS	E_0 [eV] "loose" TS
Au$_2^+$	0.65 ± 0.03	0.91 ± 0.04
Au$_3^+$	0.40 ± 0.06	0.72 ± 0.07
Au$_4^+$	0.36 ± 0.04	0.64 ± 0.04
Au$_5^+$	0.32 ± 0.09	0.57 ± 0.09
Au$_6^+$	0.20 ± 0.02	0.41 ± 0.03
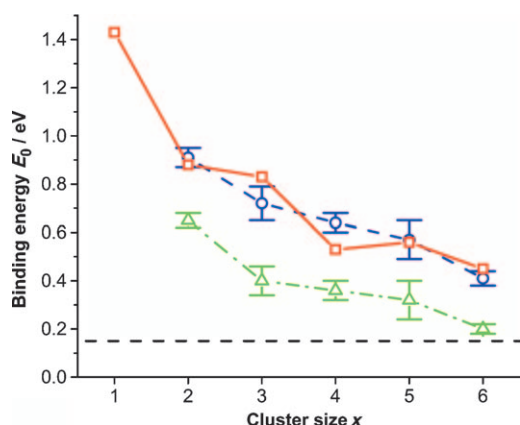
Figure 3. Cluster-size-dependent binding energies of CH$_4$ to Au$_x^+$. The blue dashed line represents the "loose" TS, the green dash-dotted line the "tight" TS and the red solid line the theoretical data. The dashed black line indicates the reported literature value for the binding energy of CH$_4$ on an extended Au(111) surface.[31]

2.4. Theoretical Results: Optimal Atomic Adsorption Geometries, Binding Energies, and Bonding Characteristics

The optimal adsorption geometries of the CH$_4$ molecule to the cation gold clusters Au$_x^+$ ($x = 1$–6), are displayed in Figure 4 along with the corresponding binding (adsorption) energies (BEs) calculated with reference to the equilibrium states of the methane molecule and the bare gold cluster cations. The in-
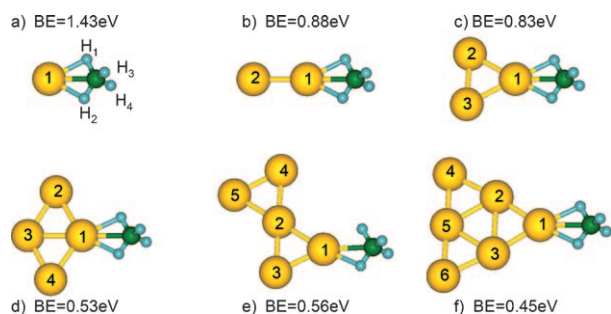
Figure 4. Calculated optimal geometries of methane adsorbed on gold cation clusters Au$_x^+$, $x = 1$–6. The methane binding energies (BE) to the clusters are given next to the atomic structures and the corresponding interatomic distances are given in Table 4. Gold atoms are depicted as yellow spheres, the carbon atom is represented by the dark green sphere, and the hydrogen atoms are described by the small blue spheres.

teratomic distances corresponding to the optimal adsorption structures are given in Table 4, and the angles in the adsorbed CH$_4$ molecule are given in Table 5. Also included in Table 4 are the interatomic distances in the bare cluster cations. The optimal structures of both the bare gold cluster cations, and after adsorption of a methane molecule, are found to be two-dimensional. In all cases the CH$_4$ molecule binds to a single gold atom of the cluster, with two of its hydrogen atoms lying in the plane of the gold cluster (see H$_1$ and H$_2$ in Figure 4) and oriented toward it, while the other two hydrogen atoms lie in the plane normal to the plane of the cluster (see H$_3$ and H$_4$ in Figure 4). The binding (adsorption) energies of the molecule to the cluster decrease as the number of atoms in the gold cluster increase (except for the gold pentamer cation where the calculated methane adsorption energy is found to be essentially the same as that for the gold tetramer cation). The calculated binding energies are in good agreement with those obtained through RRKM analysis of the experimental data employing the more realistic "loose" transition state model. The distance between the carbon atom of the methane molecule and the binding Au atom [Au(1) in Figure 4], $d_{(Au\text{-}C)}$, increases with the number of atoms in the adsorbing gold cluster (correlating with the decreasing adsorption energy), from $d_{(Au\text{-}C)} = 2.31$ Å in Au–CH$_4^+$ to $d_{(Au\text{-}C)} = 2.47$ Å in Au$_6$–CH$_4^+$ (see Table 4).

To gain insight into the nature of bonding between the gold cluster cations and the methane molecule we show in Figures 5 and 6 isosurfaces of those Kohn–Sham molecular orbitals (KSMOs) in Au$_2$–CH$_4^+$ and Au$_6$–CH$_4^+$, respectively, that have the largest amplitudes on both the gold atoms and CH$_4$ molecule (and have a bonding character, that is, do not exhibit a nodal plane between the CH$_4$ molecule and the nearest Au atom of the cluster, characteristic of anti-bonding orbitals). In each case we give the corresponding KS energy eigenvalue, and we number the KSMO from the bottom of the eigenvalue spectrum (orbital #1 being the strongly bound orbital of s-character that is localized on the hydrogen atoms). In the following we analyze the angular momentum character of a given KSMO by projecting its angular momentum (l_m) components. This is achieved via integration of the product of the KSMO with the spherical harmonic function (Y_{lm}) [repeating this procedure successively for a range of (l_m) indices, and for each angular momentum l we sum over all the m components, $-l \leq m \leq l$]; the integration is performed in a sphere of radius $4 a_0$ (where a_0 is the Bohr radius) taken about each of the atoms (the atom is located at the origin, that is, the middle of the integration sphere. For the H atoms the radius of the integration sphere is $1 a_0$). In this way we obtain an angular-momentum projected local density of states for the Au$_x$–CH$_4^+$ adsorption system under study.

Inspection of the KSMOs shown in Figure 5 for Au$_2$–CH$_4^+$ reveals two types of bonding orbitals: 1) the first type, consisting of orbitals #2 and #4, where the bonding wave function is localized on the binding gold atom [Au(1), see notation in Figure 4] and the adsorbed CH$_4$ molecule; 2) the second type, consisting of orbitals #3 and #5, where the bonding KSMO is delocalized over the entire cluster (proximal and distal gold atoms and the adsorbed methane molecule). We observe that

Table 4. Interatomic distances [Å] corresponding to the optimal geometries of Au_x–CH_4^+ clusters. $d_{(Au-Au)}$ is the distance between Au atoms (n–m), with the numbering system given in Figure 4. $d_{(Au-Au)}$ bare, gives the inter-gold distances in the bare cluster cation. $d_{(Au-C)}$ gives the distance between the binding gold atom, Au(1) and the C atom of the adsorbed CH_4 molecule. $d_{(C-H)}$ gives the distance between the carbon atom and a hydrogen atom of the adsorbed methane molecule. The H atom considered is denoted as (1) or (3); H(1) and H(2) are equivalent by symmetry, and the same holds for H(3) and H(4). In the isolated CH_4 molecule $d_{(C-H)}=1.093$ Å, and the tetrahedral angle is 109.5°.

$Au_xCH_4^+$	$d_{(Au-Au)}$ bare	$d_{(Au-Au)}$	$d_{(Au-C)}$	$d_{(Au-H)}$	$d_{(C-H)}$
$x=1$			2.31	2.07	(1) 1.14; (3) 1.10
$x=2$	2.63	2.62	2.37	2.07	(1) 1.13; (3) 1.09
$x=3$	2.65	(1–2) 2.67; (2–3) 2.61	2.42	2.10	(1) 1.12; (3) 1.09
$x=4$	(1–2) 2.68; (1–3) 2.75	(1–2) 2.72; (1–3) 2.73; (2–3) 2.65	2.48	2.14	(1) 1.12; (3) 1.09
$x=5$	(1–2) 2.69; (1–3) 2.61	(1–2) 2.73; (1–3) 2.61; (2–3) 2.65; (2–4) 2.69; (2–5) 2.70; (4–5) 2.60	2.47	(1) 2.16; (2) 2.09	(1) 1.12; (3) 1.09
$x=6$	(1–2) 2.64; (2–3) 2.89; (2–4) 2.63; (2–5) 2.76; (4–5) 2.61	(1–2) 2.64; (2–3) 2.89; (2–4) 2.64; (2–5) 2.76; (4–5) 2.61	2.47	2.15	(1) 1.12; (3) 0.92

Table 5. Angles in the adsorbed CH_4 in the optimal geometry of Au_x–CH_4^+, $x=2$–6. For numbering see Figure 4.

| x	1	2	3	4	5	6
H_1—C—H_2	126	122	120	119	118	118
H_1—C—H_3	104	105	106	106	106,107	106
H_3—C—H_4	116	114	113	113	113	113
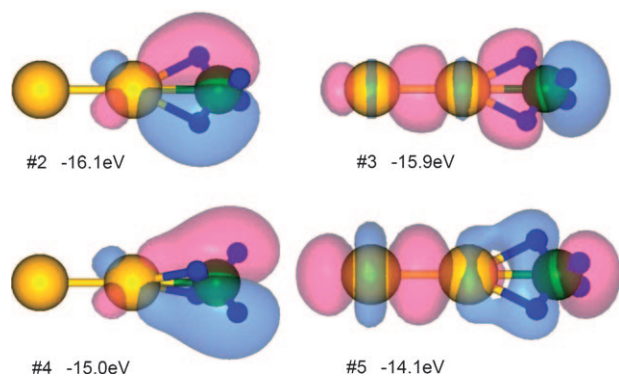
Figure 5. Isosurfaces of bonding Kohn–Sham molecular orbitals, KSMOs, superimposed on the optimal geometrical structure of Au_2-CH_4^+. The corresponding KS eigenvalues are also given. Au atoms are depicted as yellow spheres, the carbon atom is represented by the green sphere, and the hydrogen atoms are described by the small blue spheres. The pink and blue colors of the isosurfaces correspond to the positive and negative values of the wavefunctions.

the bonding KSMO with the lowest energy (#2), is (mostly) a superposition of d and p orbitals, being predominantly of d_{xz} character on Au(1) [the gold atom closest to the methane molecule], mostly of p character on the C atom (with some d-character mixed in), and having s character on the hydrogens

(recall the sp³ hybridization in the isolated CH_4 molecule). In the bonding region connecting Au(1) and C, we find contributions of mixed p and d character. The angular momentum character of KSMO #4 is similar to that of KSMO #2, with the symmetry-equivalent d_{yz} replacing d_{xz}. KSMO #3 is seen to be made of a superposition of d_{z^2} orbitals with large weights predominantly on Au(2) and Au(1) with the region around Au(1) having in addition a noticeable contribution of s character, with orbitals of p character [contributing mainly to the region around the C atom as well as the bonding region between the Au(1) and C atoms]. KSMO #5 resembles #3, but has a larger amplitude (of d_{z^2} character) on the distal gold atom, Au(2), and a relatively larger weight of p character (originating from the sp³ hybrid orbitals of the adsorbed CH_4 molecule) on the proximal, Au(1), gold atom.

Having analyzed the binding patterns for the smallest experimentally measured gold cluster cation (that is, the gold dimer), we display in Figure 6 the three bonding KSMOs for
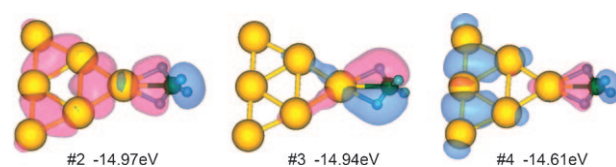
Figure 6. Isosurfaces of bonding Kohn–Sham molecular orbitals, KSMOs, superimposed on the optimal geometrical structure of Au_6-CH_4^+. The corresponding KS eigenvalues are also given. Au atoms are depicted as yellow spheres, the carbon atom is represented by the green sphere, and the hydrogen atoms are described by the small blue spheres. The pink and blue of the isosurfaces correspond to the positive and negative values of the wavefunctions.

the largest cluster system considered herein, that is, the adsorption of methane to the planar Au_6^+ cluster. Even a cursory inspection of these KSMOs reveals that one may identify in the larger system, bonding elements exhibited already in the smaller one (gold dimer). In particular, we readily recognize the two bonding orbital types identified above: type (I) where the bonding orbital is localized mainly on the binding (proximal) Au(1) atom and the adsorbed molecule, see #3 in Figure 6; type (II), consisting of KSMO #2 and #4, which are delocalized over the entire system.

The part of the lowest-energy bonding KSMO (#2 in Figure 6) of Au_6-CH_4^+ which is delocalized on the distal gold

atoms (Au(k) k = 2–6, see numbering system in Figure 4) has mostly sd character (with equal weights for the two angular momenta components), showing large amplitude in the bonding regions between the gold atoms. The part of this wave function in the neighborhood of the binding gold atom, Au(1), is also of sd character (equal weights), and the part localized on the methane molecule is predominantly of p character. The region of the bond between Au(1) and the CH_4 molecule is of mixed sd and p character. In the other type II bonding KSMO (#4) the part on the distal gold atoms is mostly of d character, with a relatively large added contribution of s character. The part localized in the bonding region between Au(1) and the adsorbed molecule is of p character (with a minority contribution of d character). In the type (I) KSMO (#3), the part localized on the CH_4 molecule is mostly of p character, and the part centered on Au(1) is mostly of d_{xz} character, with the bond region between Au(1) and the molecule being a pd hybrid.

3. Conclusions

Herein, we reported on joined theoretical simulations and gas-phase ion trap reaction kinetics of the reaction between methane and different small gold cluster cations Au_x^+ (x = 2–6). The experimental kinetic data were evaluated by fitting integrated rate equations of proposed potential reaction mechanisms to the experimental data. This not only led to the determination of reaction mechanisms for the sequential methane adsorption but also yielded temperature dependent reaction rate constants. The obtained rate constants were further analyzed by employing the Lindemann energy transfer model for association reactions in conjunction with statistical RRKM theory. This permitted, for the first time, the determination of cluster size dependent quantitative binding energy values of methane to gold cluster cations for two different transition state models. In comparison with theoretical binding energies for the optimal atomic adsorption geometries, obtained by employing first-principles density functional theory, it was shown that a "loose" transition state model represents a reasonable description of the Au_x—CH_4^+ transition state. More detailed insight into the bonding characteristics of methane to the gold cations was gained by the detailed computation of the Kohn–Sham molecular orbitals.

Acknowledgements

[1] D. K. Böhme, H. Schwarz, *Angew. Chem.* **2005**, *117*, 2388; *Angew. Chem. Int. Ed.* **2005**, *44*, 2336.
[2] T. M. Bernhardt, U. Heiz, U. Landman in *Nanocatalysis* (Eds.: U. Heiz, U. Landman), Springer, Berlin, **2007**.
[3] G. A. Olah, A. Goeppert, G. K. S. Prakash, *Beyond Oil and Gas: The Methanol Economy*, Wiley-VCH, Weinheim, **2006**.
[4] P. B. Armentrout, J. L. Beauchamp, *Acc. Chem. Res.* **1989**, *22*, 315; P. A. M. Van Koppen, P. R. Kemper, J. E. Bushnell, M. T. Bowers, *J. Am. Chem. Soc.* **1995**, *117*, 2098; Y. A. Ranasinghe, T. J. MacMahon, B. S. Freiser, *J. Phys. Chem.* **1991**, *95*, 7721.
[5] K. K. Irikura, J. L. Beauchamp, *J. Phys. Chem.* **1991**, *95*, 8344.
[6] K. Koszinowski, D. Schröder, H. Schwarz, *J. Phys. Chem. A* **2003**, *107*, 4999.
[7] K. Koszinowski, D. Schröder, H. Schwarz, *ChemPhysChem* **2003**, *4*, 1233.
[8] D. M. Cox, R. Brickman, K. Creegan, A. Kaldor, *Z. Phys. D* **1991**, *19*, 353; D. M. Cox, R. O. Brickman, K. Creegan, A. Kaldor, *Mater. Res. Soc. Symp. Proc.* **1991**, *206*, 43.
[9] S. M. Lang, T. M. Bernhardt, R. N. Barnett, U. Landman, *Angew. Chem.* **2010**, *122*, 993; *Angew. Chem. Int. Ed.* **2010**, *49*, 980.
[10] R. Keller, F. Nöhmeier, P. Spädtke, M. H. Schönenberg, *Vacuum* **1984**, *34*, 31.
[11] T. A. Miller, *J. Phys. Chem.* **1963**, *67*, 1359; R. C. Bell, K. A. Zemski, D. R. Justes, A. W. Castleman, Jr., *J. Chem. Phys.* **2001**, *114*, 798.
[12] T. M. Bernhardt, J. Hagen, S. M. Lang, D. M. Popolan, L. D. Socaciu-Siebert, L. Wöste, *J. Phys. Chem. A* **2009**, *113*, 2724.
[13] T. M. Bernhardt, *Int. J. Mass Spectrom.* **2005**, *243*, 1.
[14] L. D. Socaciu, J. Hagen, U. Heiz, T. M. Bernhardt, T. Leisner, L. Wöste, *Chem. Phys. Lett.* **2001**, *340*, 282.
[15] E. Schumacher, *DETMECH: Chemical Reaction Kinetics Software*, University of Bern, **2003**.
[16] J. I. Steinfeld, J. S. Francisco, W. L. Hase, *Chemical Kinetics and Dynamics*, 2nd ed., Prentice Hall, Upper Saddle River, **1999**.
[17] P. M. Langevin, *Ann. Chim. Phys.* **1905**, *5*, 245.
[18] S. Gilb, P. Weis, F. Furche, R. Ahlrichs, M. M. Kappes, *J. Chem. Phys.* **2002**, *116*, 4094.
[19] R. A. Marcus, *J. Chem. Phys.* **1952**, *20*, 359.
[20] K. A. Holbrook, M. J. Pilling, S. H. Robertson, *Unimolecular Reactions*, 2nd ed., Wiley, Chichester, **1996**.
[21] L. Drahos, K. Vekey, *J. Mass Spectrom.* **2001**, *36*, 237.
[22] R. N. Barnett, U. Landman, *Phys. Rev. B* **1993**, *48*, 2081.
[23] N. Troullier, J. L. Martins, *Phys. Rev. B* **1991**, *43*, 1993.
[24] H. Häkkinen, M. Moseler, U. Landman, *Phys. Rev. Lett.* **2002**, *89*, 033401.
[25] J. P. Perdew, K. Burke, M. Ernzerhof, *Phys. Rev. Lett.* **1996**, *77*, 3865.
[26] X. Ding, J. Yang, J. G. Hou, Q. Zhu, *THEOCHEM* **2005**, *755*, 9.
[27] W. E. Billups, M. M. Konarski, R. H. Hauge, J. L. Margrave, *J. Am. Chem. Soc.* **1980**, *102*, 7393.
[28] T. Shimanouchi, *Tables of Molecular Vibrational Frequencies Consolidated*, Vol. I, National Bureau of Standards, **1972**.
[29] S. M. Lang, T. M. Bernhardt, *Eur. J. Phys. D* **2009**, *52*, 139.
[30] R. E. Leuchtner, A. C. Harms, A. W. Castleman, Jr., *J. Chem. Phys.* **1990**, *92*, 6527.
[31] M. S. Wetterer, D. J. Lavrich, T. Cummings, S. L. Bernasek, G. Scoles, *J. Phys. Chem. B* **1998**, *102*, 9266.
[32] Y. Shi, V. A. Spasov, K. M. Ervin, *J. Chem. Phys.* **1999**, *111*, 938.
[33] V. A. Spasov, T. H. Lee, J. P. Maberry, K. M. Ervin, *J. Chem. Phys.* **1999**, *110*, 5208; M. F. Jarrold, J. E. Bower, *J. Chem. Phys.* **1987**, *87*, 5728.
[34] R. Marcus, *J. Chem. Phys.* **1965**, *43*, 2658.